A mathematical model of the self-averaging Pitot tube
A mathematical model of a flow sensor

Bolesław Dobrowolski, Mirosław Kabaciński*, Janusz Pospolita

Chair of Thermal Engineering and Automatic Control, Technical University of Opole, 45-233 Opole, Poland

Abstract

Flowmeters with self-averaging Pitot tubes are more and more often applied in practice. Their advantages are practically no additional flow losses, usability in the case of high temperature of fluids and simplicity of fitting. A mathematical model of a self-averaging Pitot tube including the influence of the probe shape, selected constructional features and flow conditions on the quantity of differential pressure gained has been given in this paper. The values and ranges of variations of the coefficients established for the model have been assessed on the basis of the numerically computed velocity and pressure fields around and inside the probe. Velocity and pressure fields were calculated by means of solving conservation equation and turbulence models. The characteristics linking values of the flow coefficient with values of the Reynolds number have been presented. The conclusions have been formulated taking flow metrology needs into account.
© 2005 Elsevier Ltd. All rights reserved.

Keywords: Flow measurements; Mathematical modelling; Numerical methods

1. Introduction

At present, flowmeters with tubes averaging the dynamic pressure are becoming more and more popular [1,2,12]. They seem to be better than constriction flowmeters, especially in the case of pipelines with large diameters, because they reduce or even eliminate permanent loss of pressure. Moreover, assembly costs for the flowmeters considered are much lower than for many other flowmeters. As for the flowmeters with averaging tubes, the measuring system (a converter of pressure difference, converters of pressure or temperature, a flow counter or a heat energy counter) is the same as for the constriction flowmeter.

In the literature we can find mathematical models of flowmeters, usually based on the Bernoulli equation [8] and the Euler equation, or, in some cases, on the description of a profile of the sensor considered [11]. The models allow one to determine preliminary values of the flow ratio, taking into account the profile drag coefficient of the sensor fitting, the ratio of diameters of the sensor and the pipeline (stream contraction), the roughness of the sensor surface. The models are useful for theoretical determination of metrological properties of such flowmeters; they also allow one to plan further experiments.

Because of the simplifications assumed, the models do not allow one to include complexity of the flow problems near the flowmeter and their influence on measuring characteristics of the sensor. They also do not allow one to estimate the influence of many parameters such as turbulence intensity, disturbance and velocity profile change on the coefficient K. Thus, the authors have performed numerical tests of a flow of a real fluid round the sensor based on a mathematical model using the basic equations of fluid mechanics.

While formulating the mathematical model and boundary conditions, the authors used experience and conclusions connected with modelling flows around different bodies. There are many papers on digital simulation of flows around cylinders [24–29,31]. They do not concern metrology of flows, but evaluation of usability of the standard turbulence model k–ε [26,28], physical analysis of the flow around a

* Corresponding author.
  E-mail address: kabat@po.opole.pl (M. Kabaciński).

cylinder using the vortex method [25] or evaluation of the original method of solving the equations of motion, known as the novel cut-cell Cartesian grid method [29]. In the analysis of the flow around a cylinder, special attention was paid to the variability range of the lift coefficient C_1 [18]; experimental and numerical results were compared. In [27] Spalart discussed fundamental problems of flow turbulence modelling. He presented exemplary results on the flow around a cylinder, obtained using different approaches to turbulence models. In [31], numerical pressure distributions (LES method) were compared with the experimental data and very good conformity was obtained.

From the point of view of turbulent flow modelling and the Reynolds equation, it is important to choose an appropriate model, especially in the case of flows with a high pressure gradient near the wall. In papers [14–17] we can find analysis of different turbulence models, and also variants of the k–ε model, including a comparison of the results with the experimental data. In tests, the authors also applied their own experience connected with simulation of flows through orifices [3,4,9] and other flowmeters [21,22].

The results of numerical calculations allow one to analyse velocity fields and pressure fields near the flowmeter and inside the averaging chambers. They allow one to, among other things, evaluate the influence of such parameters as the diameter of impulse holes or averaging chambers on the swellings obtained. It is also possible to formulate assumptions and suitable corrections in the mathematical model of an averaging impact tube.

2. Digital simulation of the flow near the sensor

2.1. Structures of impact flowmeters with averaging tubes

The basic element of such a flowmeter (Fig. 1) is a profile placed in the pipeline with suitable holes for pressure tapping. Differential pressure measured in the chambers inside the profile is a weighted sum of total pressures forming at the inlets of holes. The value of the effective pressure strongly depends on the number and location of holes in the sensor. Methods of selection of the number and spacing of holes are described in literature [10]. In the literature we can also find information on how to select the spacing for reduction of measurement uncertainty connected with velocity profile deformation [30] or a dirty impulse hole (a change of the section area) [13].

The relationship between the mean fluid velocity in the pipeline section and the measured differential pressure is

$$w = K \sqrt{\frac{2\Delta p}{\rho}} \qquad (1)$$

where $\Delta p = p^+ - p^-$ is the difference of pressures at the ends of the averaging chambers, ρ is the fluid density, K is the flow coefficient. The equation is similar to the relationship between the flux and pressure difference in
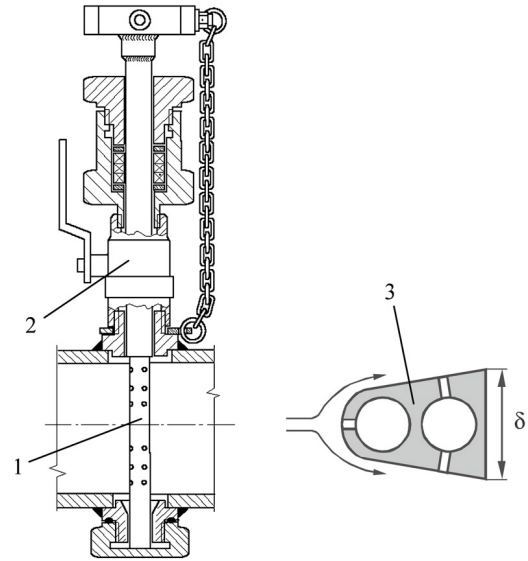

Fig. 1. Structure of a flowmeter with the impact flow sensor: 1—averaging impact tube, 2—cut-off valve, 3—cross section of the tube with marked averaging chambers.

the case of constriction flowmeters. The main difference is connected with the swells obtained (Δp). In the case of constriction flowmeters, swells are usually greater and the flow coefficient K is of a more nonlinear character (especially for the lower Reynolds numbers).

The sensor profile strongly influences the pressure difference. A sensor of a given profile should give the highest possible swells and constant flow ratio and reduction or elimination of the measuring signal pulsation. Some firms have proposed some interesting solutions—their flowmeters have advantages typical for a given type and their faults are reduced so it is possible to obtain relatively precise measurements.
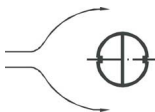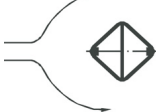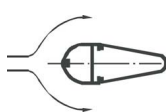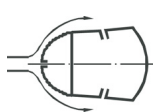
Table 1 shows sections of the sensors applied in the flowmeters. Information about the swells obtained is also given.

The values given for the coefficient K for the sensors presented are the average values resulting from the sensor shape. They do not include the sensors in the pipelines with small diameters. Then low values of K, for example 0.4, result from the flow swelling on the sensor, like in the constriction flowmeter.

2.2. The flow system considered

The sensor with air flowing round was considered. Its section is shown in Fig. 1 [20]. Such a section allows one to obtain a very low variation of the flow ratio K over a wide range of the Reynolds numbers [10]. Tapping of pressure p^+ (higher pressure) takes place on the profile face and of p^- (lower pressure) on the lateral surfaces, near trailing edges. Inside the sensor there are the chambers averaging the pressure (see Fig. 1). Flows inside and around the sensor located in the pipeline were tested. The flow around the

Table 1
Sections of sensors applied in the flowmeters

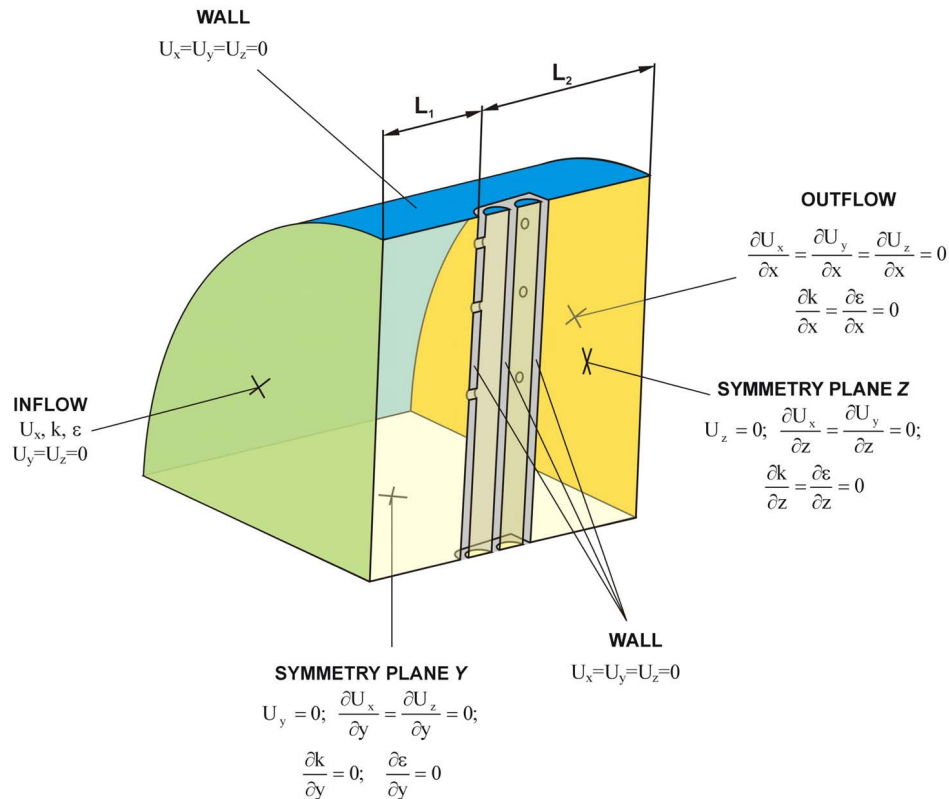| Section of sensor					
K	0.6–0.7	0.6–0.65	0.7–0.8	~ 0.7	~ 0.6
$\frac{\Delta p}{\frac{\rho w^2}{2}}$	2–2.8	2.4–2.8	1.6–2	~ 2	~ 2.8

Fig. 2. A part of the flow system considered with the boundary conditions (sensor with a streamline section).

sensor of a uniform free stream (a two-dimensional problem) was also considered.

Fig. 2 shows the flow system considered. For better efficiency of calculations – taking into account the symmetry of the system – we considered only a quarter of the flow area. We assumed suitably long inlet and outlet intervals, motivating the assumed boundary conditions in the inlet and outlet sections. Fig. 2 also contains the assumed boundary conditions. At the inlet the profiles of velocity U_x, kinetic energy of turbulence k and its dissipation velocity ε were introduced. These profiles had been obtained by simulation of air flow in pipelines with different diameters, suitable for each case. A suitable length of the pipeline was chosen ($l = 40D$, where l is the pipeline length and D is its diameter), for which the above-mentioned profiles were stabilized; i.e., increase of the ratio of the pipeline length

to its diameter did not influence the results obtained. The velocity profile agrees with theoretical assumptions based on Nikuradse's tests for different Reynolds numbers [23].

2.3. Mathematical model of the flow

In this paper a mathematical model of the flow in the averaging impact tube has been formulated. A turbulent stationary flow of a viscous incompressible fluid is considered. The fluid (in this case air) was assumed incompressible because of the assumed velocity range 6–30 m/s (much lower than the speed of sound). In such conditions assuming incompressibility does not cause important errors. The mathematical model for a 3-D case is

based on the transport equation

$$\frac{\partial(\rho\overline{U}_i\overline{U}_j)}{\partial x_j} = -\frac{\partial p}{\partial x_i} + \frac{\partial}{\partial x_j}\left[\mu_{\text{ef}}\left(\frac{\partial\overline{U}_i}{\partial x_j} + \frac{\partial\overline{U}_j}{\partial x_i}\right)\right], \qquad (2)$$

and the equation of continuity

$$\frac{\partial(\rho\overline{U}_i)}{\partial x_i} = 0. \qquad (3)$$

In the above equations $\overline{U}_i$ is a component of the velocity vector in direction x, y or z, p is the pressure, ρ is the fluid density. μ_{ef} is the effective viscosity, a sum of molecular μ and turbulent μ_t viscosities; i.e.,

$$\mu_{\text{ef}} = \mu + \mu_t. \qquad (4)$$

Turbulent viscosity is determined from a standard turbulence model, k–ε:

$$\mu_t = C_\mu \frac{k^2}{\varepsilon} \qquad (5)$$

where $C_\mu = 0.09$ for the standard k–ε model for developed turbulence. The kinetic energy of the turbulence k and its dissipation ε are determined from the following transport equations:

$$\overline{U}_i \frac{\partial k}{\partial x_j} = \frac{1}{\rho}\frac{\partial}{\partial x_j}\left(\frac{\mu_t}{\sigma_k}\frac{\partial k}{\partial x_j}\right)$$
$$+ \frac{\mu_t}{\rho}\left(\frac{\partial\overline{U}_i}{\partial x_j} + \frac{\partial\overline{U}_j}{\partial x_i}\right)\frac{\partial\overline{U}_i}{\partial x_j} - \varepsilon \qquad (6)$$

$$\overline{U}_i \frac{\partial\varepsilon}{\partial x_j} = \frac{1}{\rho}\frac{\partial}{\partial x_j}\left(\frac{\mu_t}{\sigma_\varepsilon}\frac{\partial\varepsilon}{\partial x_j}\right)$$
$$+ \frac{C_1\mu_t\varepsilon}{\rho k}\left(\frac{\partial\overline{U}_i}{\partial x_j} + \frac{\partial\overline{U}_j}{\partial x_i}\right)\frac{\partial\overline{U}_i}{\partial x_j} - C_2\frac{\varepsilon^2}{k}. \qquad (7)$$

The system of equations was completed with boundary conditions suitable for the three-dimensional problem considered (Fig. 2). The equations of the mathematical model were solved numerically and velocity and pressure fields were determined for the stream flowing round the tube and inside the averaging chambers.

It is very important to formulate suitable initial conditions influencing accuracy of calculations and the time necessary for them. The necessary initial values of U_x, k and ε at the inlet should be declared, taking into account all the section points (their number is dependent on the mesh density). They can be obtained from the empirical data or from numerical calculations which can be realized at two stages because of the computer resources. The first stage includes digital simulation of an air flow in the empty pipeline of a length allowing for stabilization of profiles U_x, k and ε (about 40 to 60 diameters depending on the Re number characterizing the flow). At the other stage we apply the profiles obtained as boundary conditions and the initial conditions at the inlet of the flow system considered. The calculations begin at the inlet and they are continued to the outlet until the declared convergence (in this case 10^{-4}) is reached.

The standard turbulence model, k–ε, can be used only for fully turbulent flows—this means that the influence of molecular viscosity is insignificant [5].

Boundary conditions at the inlet determine the profiles U_x, k and ε. The velocity vector components on the walls are equal to zero. In order to increase the accuracy of calculations (because of limited computer resources), the authors used the symmetry of the system in two directions, y and z, and declared boundary conditions for both planes. On the symmetry plane, the component of the velocity vector normal to the plane as well as the gradients of the remaining quantities shown in Fig. 2 are equal to zero. At the outlet the Neumann boundary condition was used, i.e. the gradients for u, k and ε were equated to zero.

Boundary conditions for the walls resulted from the applied version of the turbulence model. The velocity vector components U_x, U_y, U_z are equal to zero.

2.4. Results of calculations

Equations for the mathematical models were solved with the finite volume method and the FLUENT software [5]. Discretization of the calculation area was done with the GAMBIT program [6]. A non-structural mesh based on tetrahedral elements was applied. The number of mesh elements was about 2 million cells; i.e., in the calculation method considered, about 0.5 million nodes at which solutions of the system of equations were determined (2), (3), (6) and (7).

A fluid flow was subjected to simulation for velocities from 6 to 30 m/s, i.e. with a Reynolds number in the range $6.2\times10^4 < Re < 3.1\times10^5$ relating to the pipeline diameter. This corresponds to a range of the Re_δ number related to the sensor width δ ($5.8\times10^3 < Re_\delta < 2.9\times10^4$). Moreover, for calculations, we assumed: $D = 25$–200 mm (pipeline diameter), $d = 10$ mm (sensor diameter in the case of circular section), $\delta = 13.6$ mm (width of the sensor with the streamline section), $n = 4$ and 6 (number of impulse holes on the sensor wall), $\rho = 1.225$ kg/m^3, $L_1 = 40$–$60D$ (length of the straight interval of the pipeline before the sensor) and $L_2 = 5D$ (length of the straight interval of the pipeline behind the sensor). L_1 and L_2 are shown in Fig. 2. The turbulence intensity of the air stream at the inlet was assumed as $i \approx 6\%$, and it is a typical value (5%–10%) for a great number of complex flow problems [5].

Fig. 3 shows the calculated velocity and pressure fields in the horizontal symmetry plane of the flow system. As for pressure, its distribution on the pipeline wall was also presented in the case of the velocity profile—on the wall the vector u is equal to zero, according to the boundary conditions.

The influence of the sensor on the flowing fluid stream can be observed (Fig. 4). In spite of the streamline shape and small dimensions, the sensor influences the stream. The pressure distribution with a big zone of negative pressure is especially interesting (Fig. 4(b)).
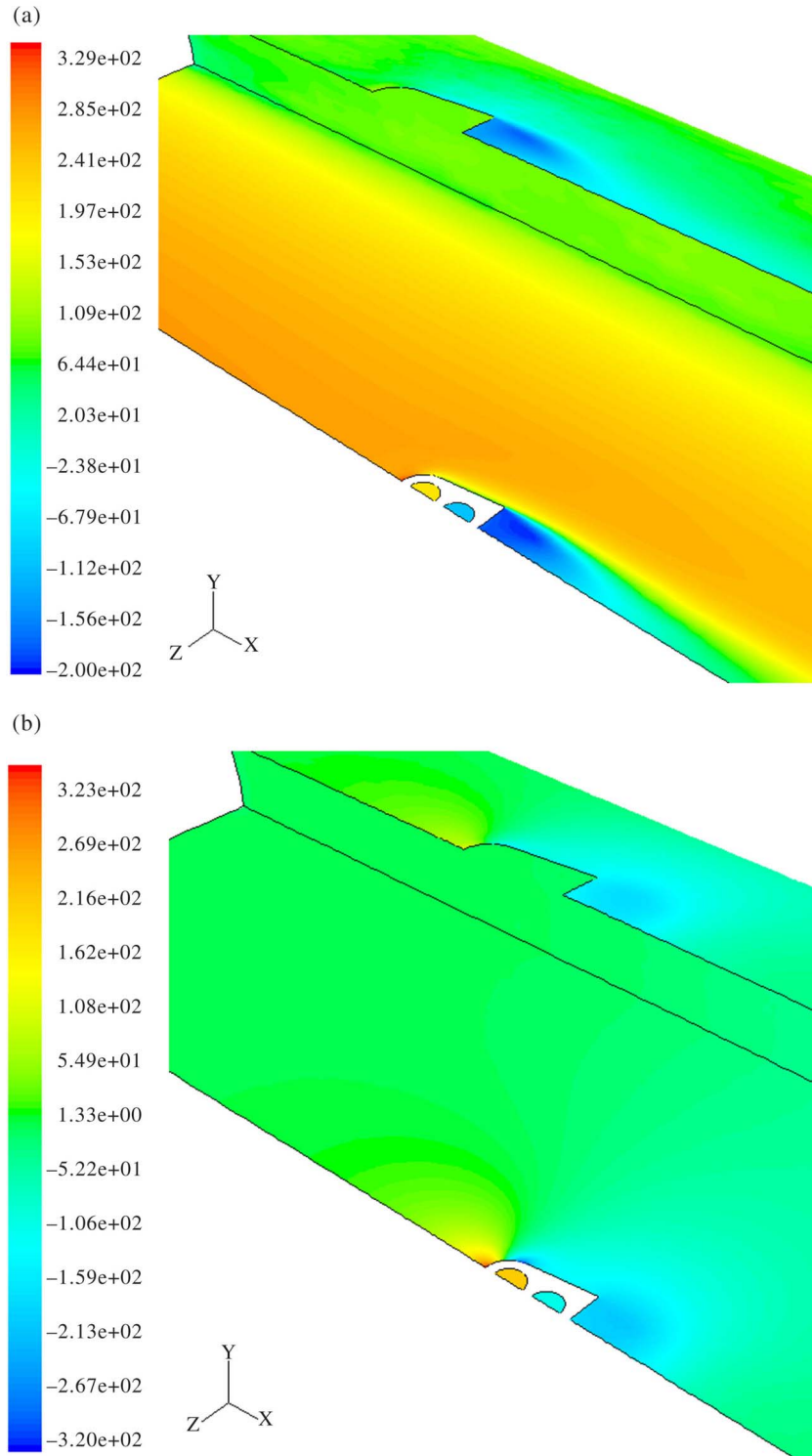
Fig. 3. Distribution of component U_x of the vector (a) and static pressures (b) for a sensor with the streamline section for the mean velocity 18 m/s.

Fig. 5 shows a map of total pressures around the sensor. The pressure distribution at the face is typical because of the existing velocity profile (dynamic pressure, in the second power dependent on velocity, is dominating) in the pipeline.

Fig. 6 shows the total pressure distribution inside the averaging chambers of the sensor. It should be observed that

in spite of the variable pressure around the impulse holes of the profile surface at the face and lateral surface, the pressure inside the chambers is almost homogeneous (see Fig. 7).

Fig. 7 presents pressure distributions inside the averaging chambers and velocities in the hole sections for three selected mean velocities, 10, 14 and 18 m/s. Because of
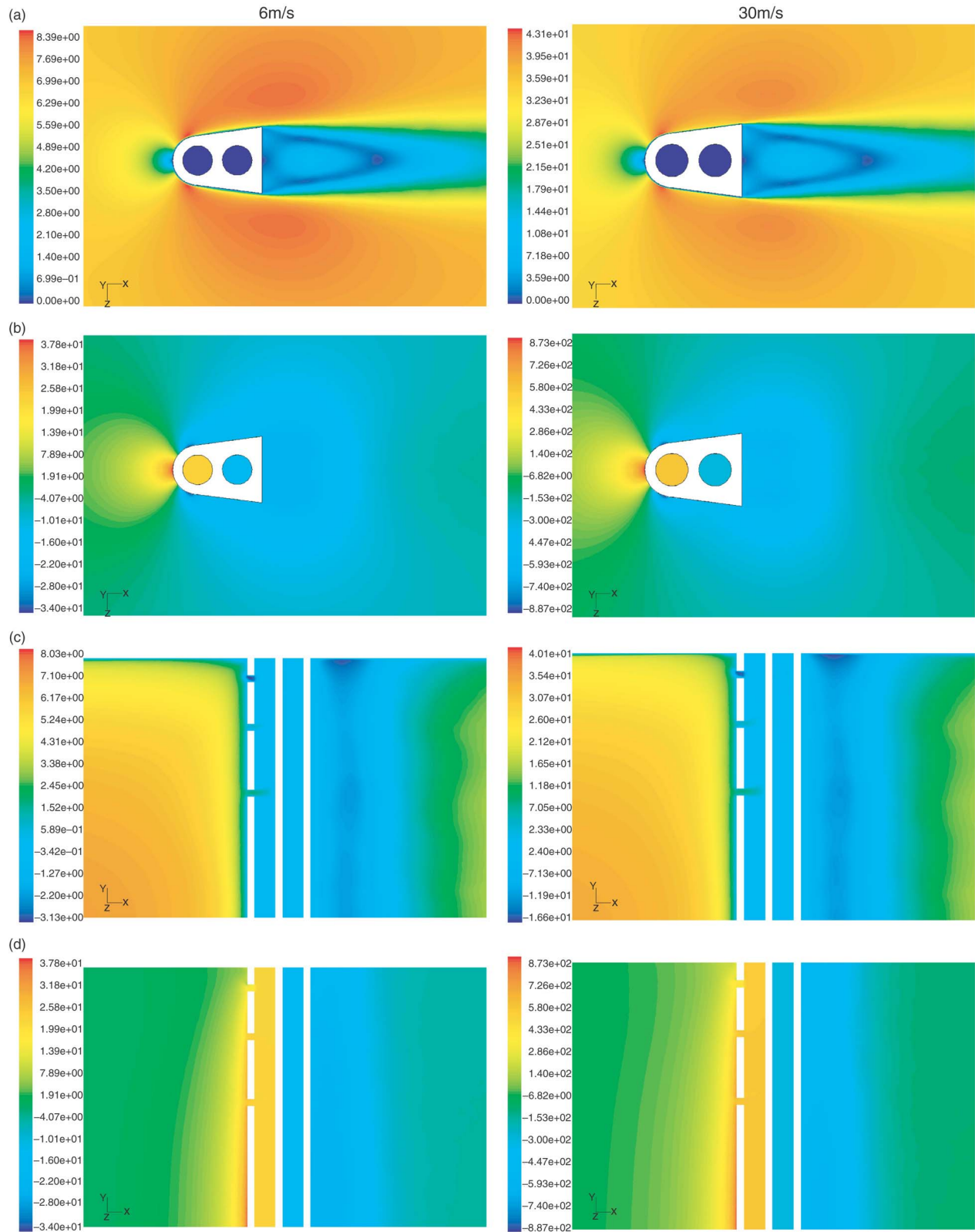
Fig. 4. Distribution of axial velocity component x ((a), (c)) and static pressures ((b), (d)) in the horizontal and vertical planes of symmetry, respectively, for two extreme mean velocities, 6 and 30 m/s.

similarity and easier visualization of pressure distributions inside the chambers and velocities inside the impulse holes, the results were presented for the sensor with a circular section. The pressure distributions presented for inside
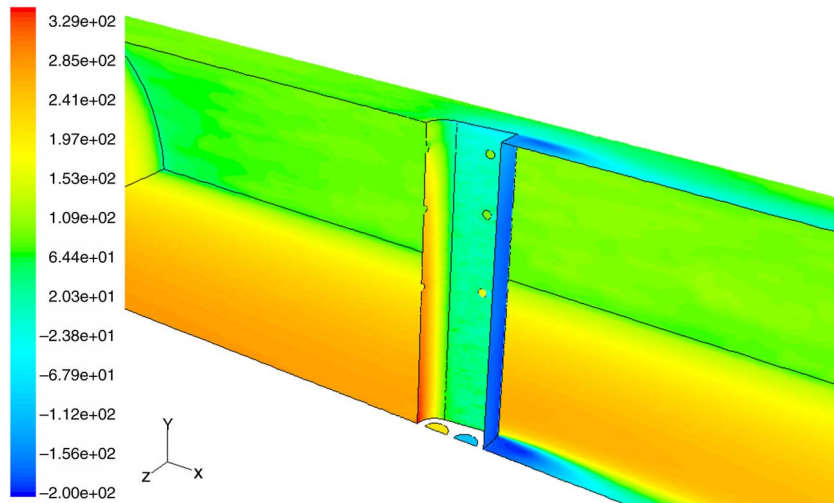
Fig. 5. Total pressure distribution around the sensor with a streamline shape for the mean velocity 18 m/s.
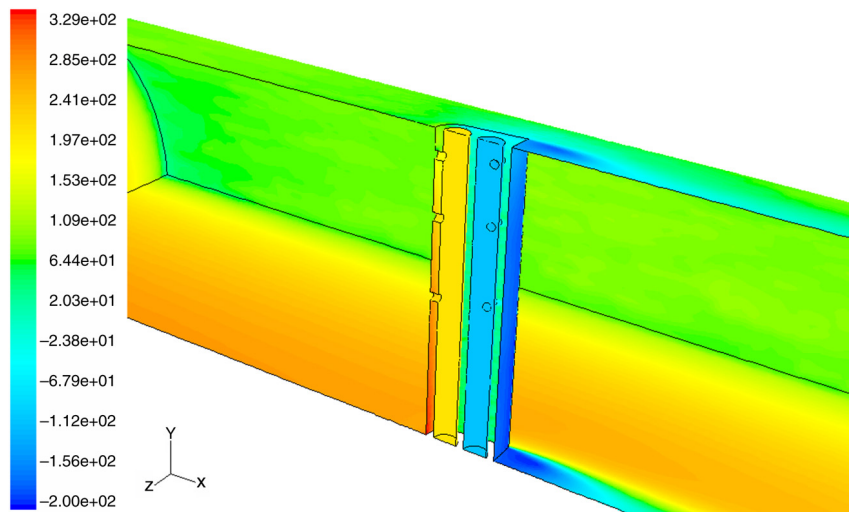

Fig. 6. Total pressure distribution inside the averaging chambers for the mean velocity 18 m/s.

the chambers are slightly diversified in spite of the high gradients of these values outside the probe. Inside the first chamber (p^+) we can observe recirculation of the medium which flows in through two holes located near the pipeline axis (causing the total pressure increase near these holes) and flows out through the hole nearest to the pipeline wall causing the medium recirculation effect. At the other side, recirculation in the chamber is less intense and the pressure distribution is almost homogeneous, so only one impulse hole could be applied on this side.

Fig. 8 shows the influence of the averaging chamber size on pressure averaging inside the chambers for a small section area. The selected chamber diameter is the same as the impulse hole diameter (2 mm) because of the dissimilarity of the flow phenomena and a worse pressure averaging at this geometry. The chamber diameter is equal to $\frac{1}{3}$ of the diameter of the averaging chamber of the sensor subject to the above considerations. In this case

we can observe an excessive tendency of the medium to recirculation in some directions. For the mean velocity 18 m/s, the pressure variability along the chamber p^+ is about 80 Pa, i.e. 59% the mean value. The results obtained make the flowmeter interior design easier and allow one to know mistakes of possible structures without expensive tests. In the case considered, the drop of the difference between the pressures measured at the chamber ends (where the pressure difference converter is located) and their non-uniform distribution inside the chamber are unfavourable.

3. Mathematical model of the flow sensor

An averaging impact tube is shown in Fig. 9. The figure also presents a way of effecting velocity marking before the holes, in the area undisturbed by the sensor and the pressures, in the sections of impulse holes on the two sides
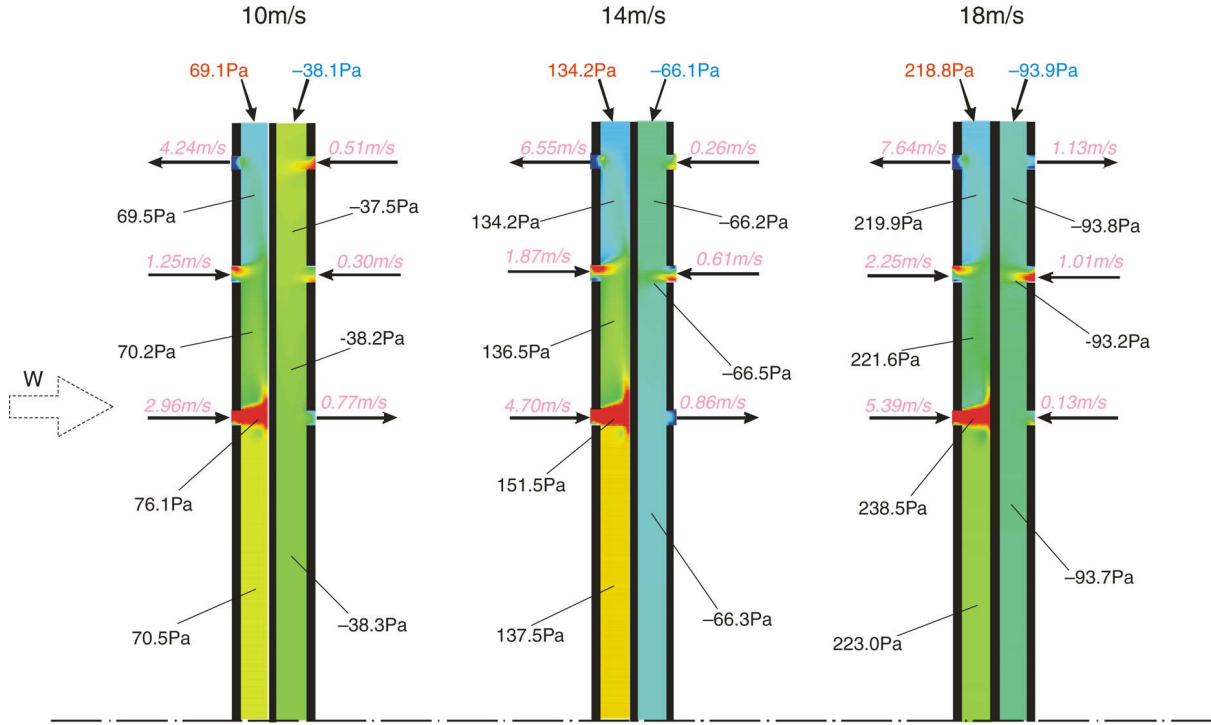
Fig. 7. Pressure distributions at characteristic points inside the chambers and velocities in the impulse holes for three selected mean velocities.

of the sensor. The pressure difference between the averaging chambers (received at the end) is a measuring signal.

A relation between the mean flow velocity in the section and the differential pressure has been discussed in 2.1 (Eq. (1)).

In the sensor design it is assumed that the mean pressure in the chamber is the average of the total pressures in the sections of the impulse holes on two sides, p_{in} and p_{io}:

$$p^+ = \frac{1}{k} \sum_{i=1}^{k} p_{in} \tag{8}$$

and

$$p^- = \frac{1}{k} \sum_{i=1}^{k} p_{io} \tag{9}$$

where k is the number of holes. In [7,30] the methods of impulse hole location are presented. The pipeline section is often divided into coaxial rings with the same areas. Pressure is received at points located on the circles dividing areas of the rings into halves:

$$r_i = R\sqrt{\frac{2i-1}{2k}} \tag{10}$$

where $2k$ is the number of holes in the averaging tube, i is the number of successive holes from the pipeline axis. Velocities at the points located at the two ends of the radii with lengths resulting from Eq. (13) are not equal to the mean velocities, so the radii with the holes at their ends are often determined in another way. The following velocity

distribution expressed as a Prandtl equation is assumed:

$$U_x = U_{xo} \left(1 - \left(\frac{r}{R}\right)\right)^{\frac{1}{m}} \tag{11}$$

where U_{xo} is the velocity in the pipeline axis and m is an exponent dependent on the Reynolds number. For example, for the Reynolds numbers considered ($Re = 6.2 \times 10^4$–3.1×10^5), $m = 7$–8. Using the velocity profile determined from the above equation, we can determine the mean velocity in the ring and the radius where the mean velocity is equal to the local velocity. The radii determined for particular rings show how the impulse holes should be located. If the k-th ring is limited by the circles with radii r_{k1} and r_{k2} derived from

$$r_{ki} = R\sqrt{\frac{i}{k}} \tag{12}$$

where k is the number of holes in the averaging tube (being half of the total number of holes on one side of the sensor) and i is used for numbering successive holes from the pipeline axis; then the position of the impulse hole is expressed by the following equation [30]:

$$r_i = \left(\frac{2(r_{i2}^{m+2} - r_{i1}^{m+2})}{(m+2)(r_{i2}^2 - r_{i1}^2)} \right)^{\frac{1}{m}}. \tag{13}$$

The exponent m is assumed for the nominal flow. In the case of variable flow it can cause some errors (see Table 2).

Methods of determination of such errors are based on comparison of the numerical mean velocity at the inlet with the mean velocity determined from some representative
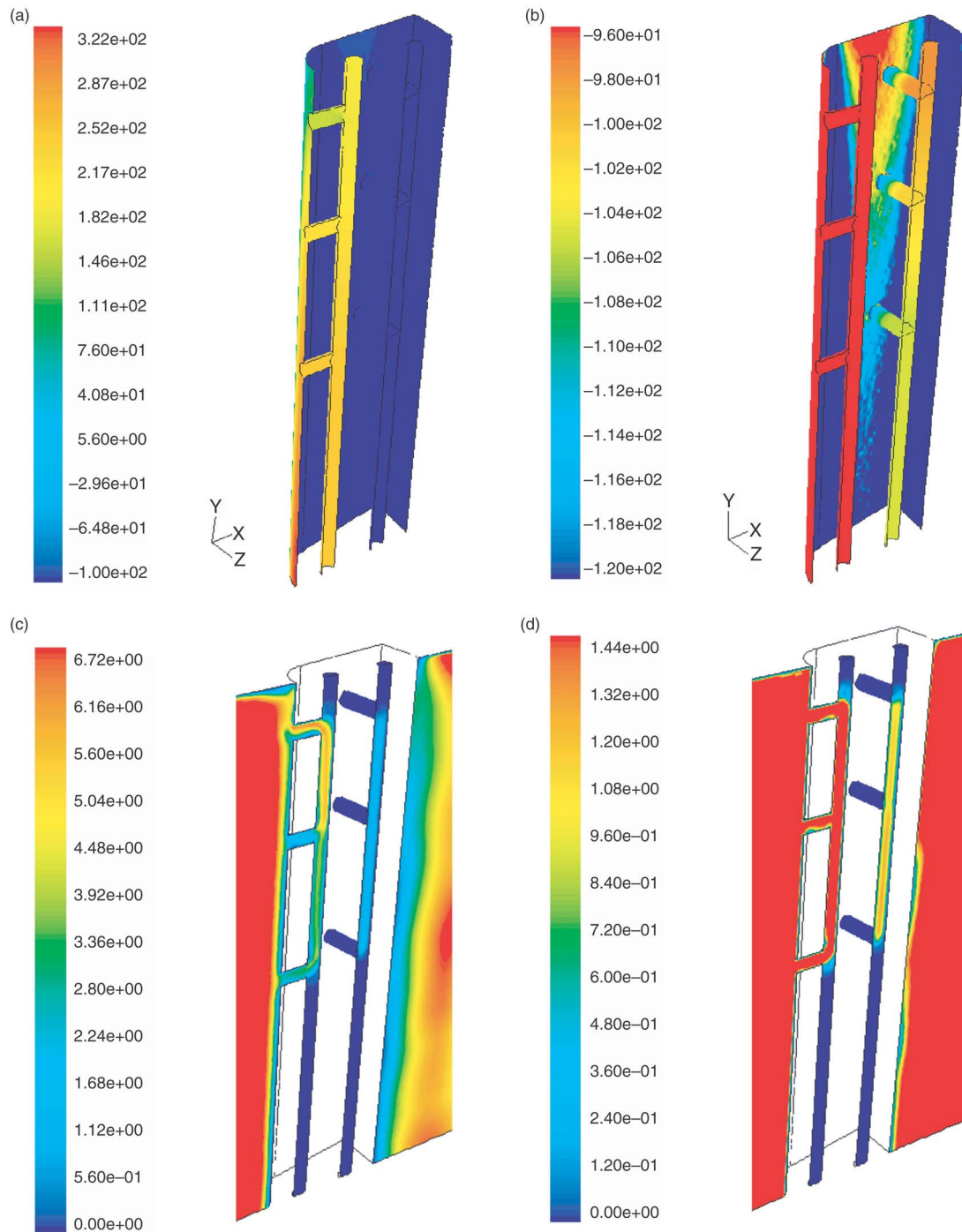
Fig. 8. Distribution of pressures ((a), (b)) and velocities (c) in the chamber, p^+, (d) in the chamber, p^-, inside the averaging chambers of the sensor of the streamline profile (chambers 2 mm in diameter) for $U_x = 18$ m/s.

points corresponding to hole positions in the sensor. Various positions of the representative points within the pipeline diameter dependent on the exponent m have been presented for the sensors with four and six holes. As the Reynolds number rises, the velocity profile takes a form corresponding to the profiles with higher exponents m. The hole locations were determined for $m = 8$, which is the best for the velocity profile in the range of Re numbers considered.

In the case of a sensor with a tube averaging dynamic pressure, the flow coefficient K results from the sensor profile K_1, a correction including nonlinearity between the velocity and dynamic pressure K_2, the blockage effect of the sensor on the fluid stream in the pipeline K_3 [12] and possible corrections connected with hole arrangement K_4 and for higher flow velocities, including the compressibility K_5:

Table 2
Measuring errors connected with the hole location in the sensor

Number of holes	Hole arrangement		Error [%] for Re		
			6.16×10^4	1.85×10^5	3.08×10^5
4	According to Eq. (14)	$m = 7$	−0.23	−0.06	0.05
		$m = 10$	0.69	0.71	0.75
		$m = 13$	2.42	2.18	2.09
	According to Eq. (11)		−2.34	−1.90	−1.66
6	According to Eq. (14)	$m = 7$	−0.43	−0.90	−0.20
		$m = 10$	0.00	0.09	0.15
		$m = 13$	1.41	1.70	1.10
	According to Eq. (11)		−2.25	−1.86	−1.66

$$K = K_1 \cdot K_2 \cdot K_3 \cdot K_4 \cdot K_5. \qquad (14)$$

A coefficient including the sensor profile can be determined from analysis of its flow with a plane unlimited stream. The coefficient joins the pressure difference at the assumed profile points where pressure is received with the flow velocity in the undisturbed area. Figs. 10 and 11 show values of K_1 for the sensor with a circular and streamlined profile versus the Reynolds numbers.

Nonlinearity between dynamic pressure and flow velocity can be taken into account in the following way. The local flow velocity (in the hole plane on both sides) can be written as

$$w_i = K_1 \sqrt{\frac{2}{\rho}(p_{\text{in}} - p_{\text{io}})}. \qquad (15)$$

It is assumed that the flow resistance in the pipeline caused by the sensor (for the diameters of the pipeline and the sensor considered) can be neglected. Fluid compressibility was neglected for the reasons mentioned in Section 2.3. The rings and points of pressure reception are chosen such that

$$w = \frac{1}{k} \sum_{i=1}^{k} w_i. \qquad (16)$$

Introducing (15) to (16) we have

$$w = K_1 \sqrt{\frac{2}{\rho}} \frac{1}{k} \sum_{i=1}^{k} \sqrt{(p_{\text{in}} - p_{\text{io}})}. \qquad (17)$$

Because

$$w = K_1 K_2 \sqrt{\frac{2}{\rho}} \sqrt{\frac{1}{k} \sum_{i=1}^{k} p_{\text{in}} - \frac{1}{k} \sum_{i=1}^{k} p_{\text{io}}}, \qquad (18)$$

K_2 can be expressed as

$$K_2 = \frac{\frac{1}{k} \sum_{i=1}^{k} \sqrt{(p_{\text{in}} - p_{\text{io}})}}{\sqrt{\frac{1}{k} \sum_{i=1}^{k} p_{\text{in}} - \frac{1}{k} \sum_{i=1}^{k} p_{\text{io}}}}. \qquad (19)$$
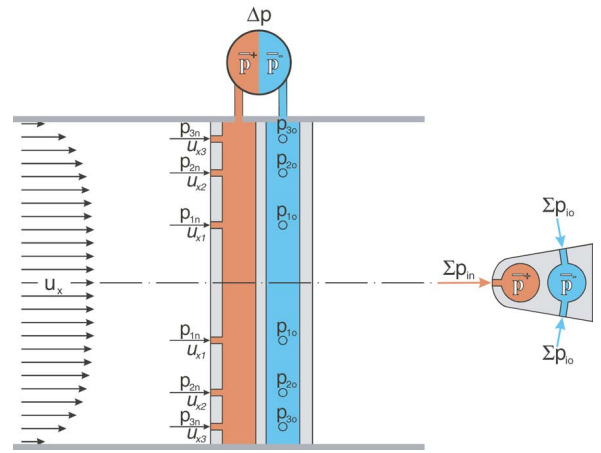

Fig. 9. Principle of operation of the averaging impact tube.

Fig. 12 shows K_2 versus Re numbers for the sensors with four and six holes. The values of K_2 demonstrate that the impulse holes are well distributed in the sensor. Moreover, there is a low difference between the values of K_2 for two sensors with different numbers of holes and the sensor with a low number of holes seems to be a better one.

The coefficient K_3 including the blockage effect of the sensor can be determined from analysis of the pressure difference Δp for a sensor located in the pipeline when $D \gg d$, where d is the diameter of a round sensor or the thickness of a streamlined sensor and a sensor located in the pipeline of lower diameter. Comparison needs the same mean flow velocities. If the influence of the Re number on K_1 is strong, we have to take this fact into account in calculations. Thus, we can determine K_3 from

$$K_3 = \frac{K_1}{K_{1D}}, \qquad (20)$$

where D means the quantities are considered for the flow in a pipeline of large diameter, i.e. $D \gg d$.

Fig. 13 shows values of K_3 for the sensor considered versus the pipeline diameter. The values shown illustrate the influence of the pipeline diameter on the pressure difference
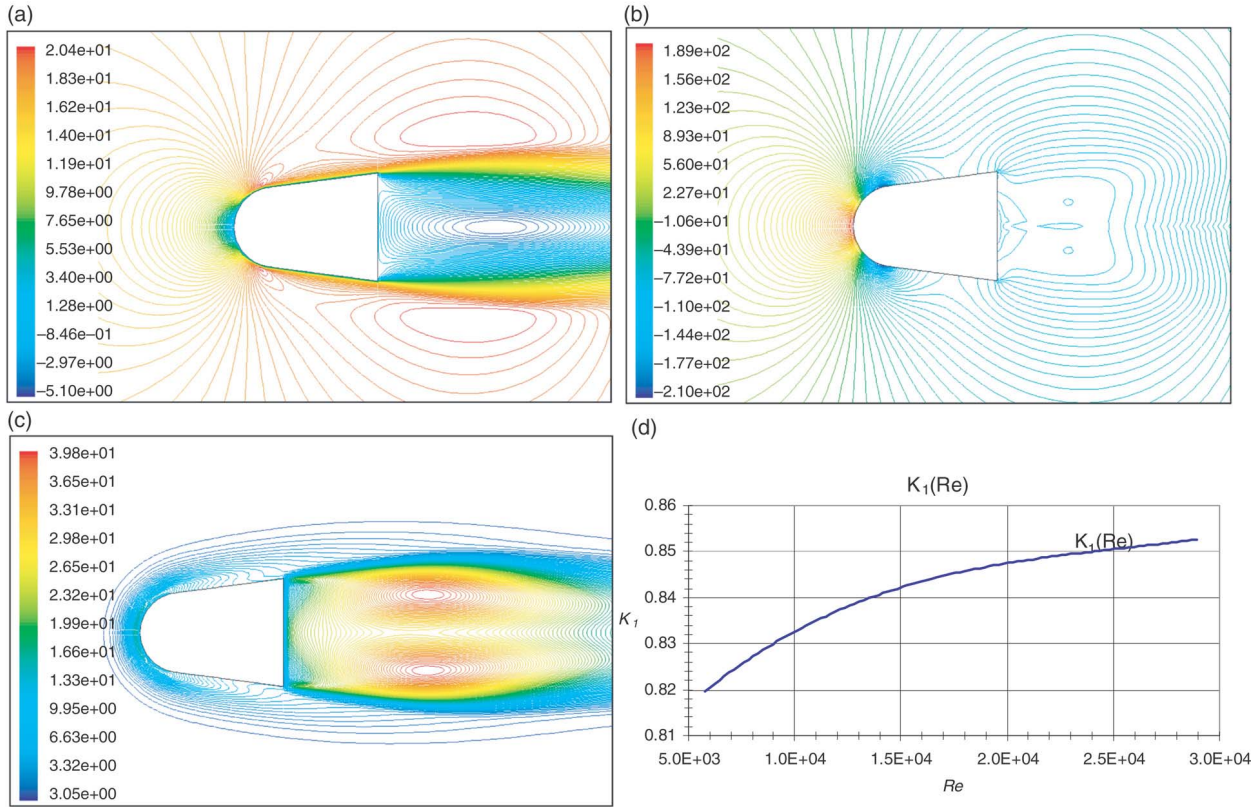
Fig. 10. Distributions of velocity (a), static pressure (b) and kinetic energy of turbulence (c) around the sensor located in a homogeneous air stream with velocity 18 m/s and coefficients K_1 versus Re number (d).

obtained on the sensor and on the ratio of the K-factor in the pipeline with a smaller diameter K_1 to K_{1D} in the pipeline with a big diameter ($D \gg d$). From the graph it appears that the influence of the pipeline wall is not significant when the diameter is greater than 125 mm.

The coefficient including a system of holes in the sensor can be determined for example from the data included in Table 2. It can be a correction given versus the Re number or a value including a difference, when they are related to the values obtained from Eq. (13). Fig. 14 includes example values of K_4, for holes made according to Eq. (12).

It can be observed that for sensors with six and more holes on each side and for higher Re numbers, K_4 is close to one and it does not strongly influence the flow ratio of the sensor. Individual calibration of the sensor in the pipeline allows one to obtain the characteristics $K = f(Re)$ in general, including the sensor shape, stream blockage, nonlinearity between dynamic pressure and flow velocity as well as methods of hole making.

Values of the compressibility coefficient K_5 can be determined according to the equations known from the literature, for example [30]

$$K_5 = \left[1 + \frac{Ma^2}{4} + (2 - \kappa) + \frac{Ma^2}{24} + \cdots \right]^{-1} \qquad (21)$$

where κ is an exponent of the gas adiabat and Ma is the Mach number, equal to

$$Ma = \frac{w}{\sqrt{\frac{\kappa \cdot p_s}{\rho}}}. \qquad (22)$$

For liquids, $K_5 = 1$. For gas flows, when $Ma \ll 1$, it can also be equal to 1.

Fig. 15 shows the influence of the velocity w of the flowing medium on the measuring error Δw expressed in m/s. For velocities used in the simulation (6–30 m/s), the influence of air compressibility can be neglected. However, above 40 m/s that influence becomes significant for measurements of velocity. For 70 m/s ($M = 0.2$) the measuring error for dynamic pressure is 1.0%, and for the velocity it is 0.5% [19].

4. Characteristics of sensors

Fig. 16 presents characteristics of the sensors considered. The streamline sensor has a higher, unfavourable flow ratio K, but the characteristic is flatter. Thus, it is possible to accept stability of K over a wider range of the Reynolds number variation. It is interesting that for low flow velocities the characteristic is strongly nonlinear and the value of its K-factor decreases. In this case it is possible to include changes $K = f(Re)$ in the measuring system or use the possibilities
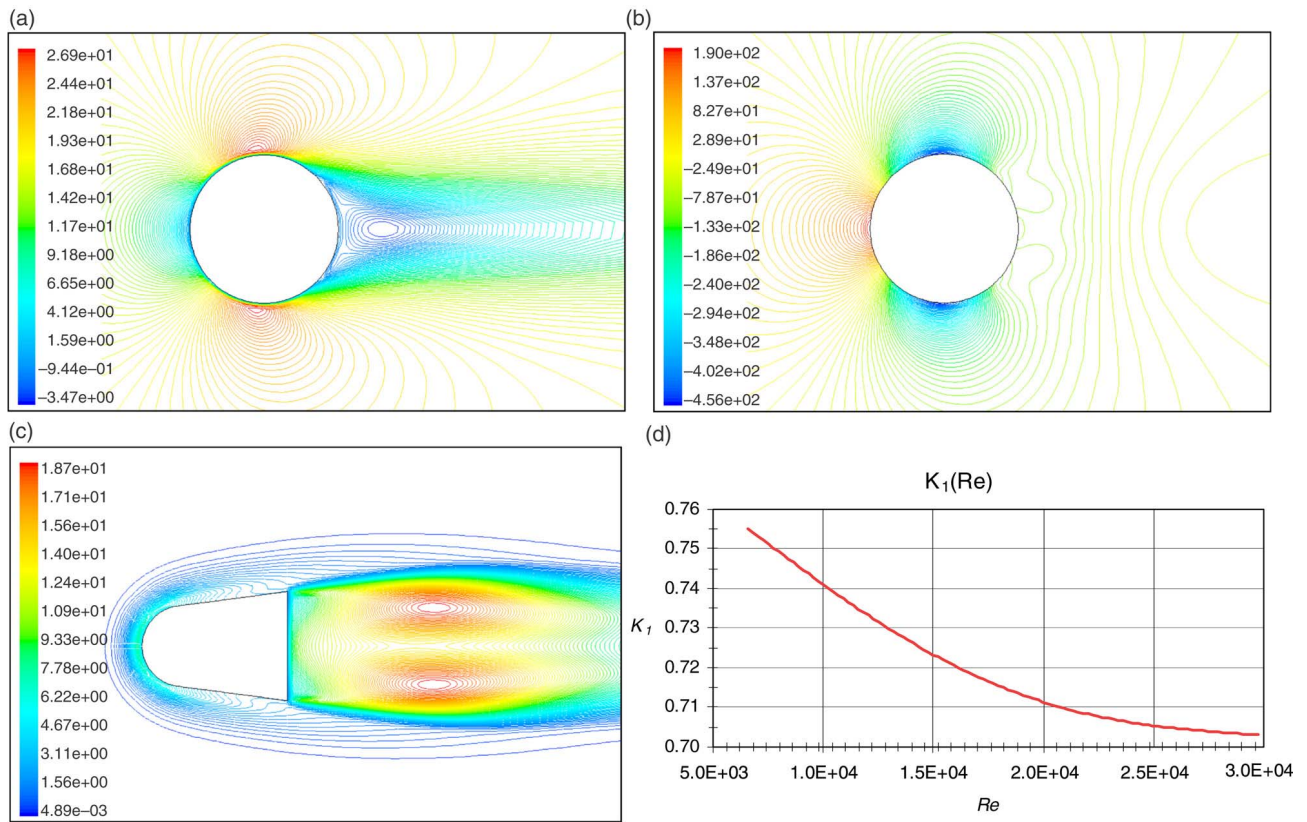
Fig. 11. Distributions of velocity (a), static pressure (b) and kinetic energy of turbulence (c) around the sensor with circular section located in a homogeneous air stream with velocity 18 m/s and coefficients K_1 versus the Reynolds numbers (d).
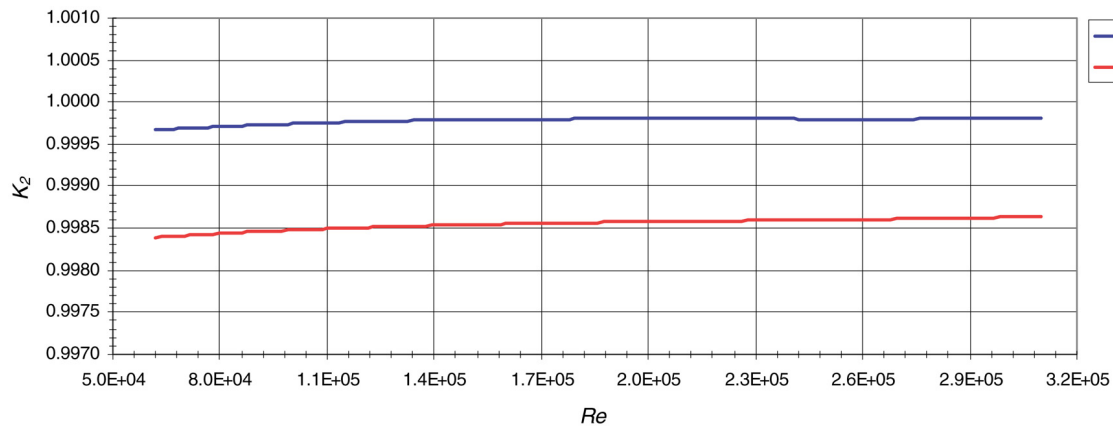

Fig. 12. Values of K_2 for sensors with four and six holes.

of modern converters of pressure difference, for example by formulation of 16-point characteristics. From calculations it appears that K is strongly influenced by sensor shape and its blockage effect on the flowing stream. This result is found from values of K_1 and K_3 in Figs. 10 and 13 respectively.

The sensor characteristic is not so strongly dependent on the number and location of holes. The holes should be located according to Eq. (13). It is also possible to place them near the central flow area in order to enlarge the measuring pressure drop and individual calibration of the sensor. Fig. 16 presents the characteristics $K = f(Re)$ for sensors with different hole systems. Calculations were also made for a sensor with one impulse hole at the outlet side, where K is lower and more favourable.

(a)

(c)

(b)

(d)

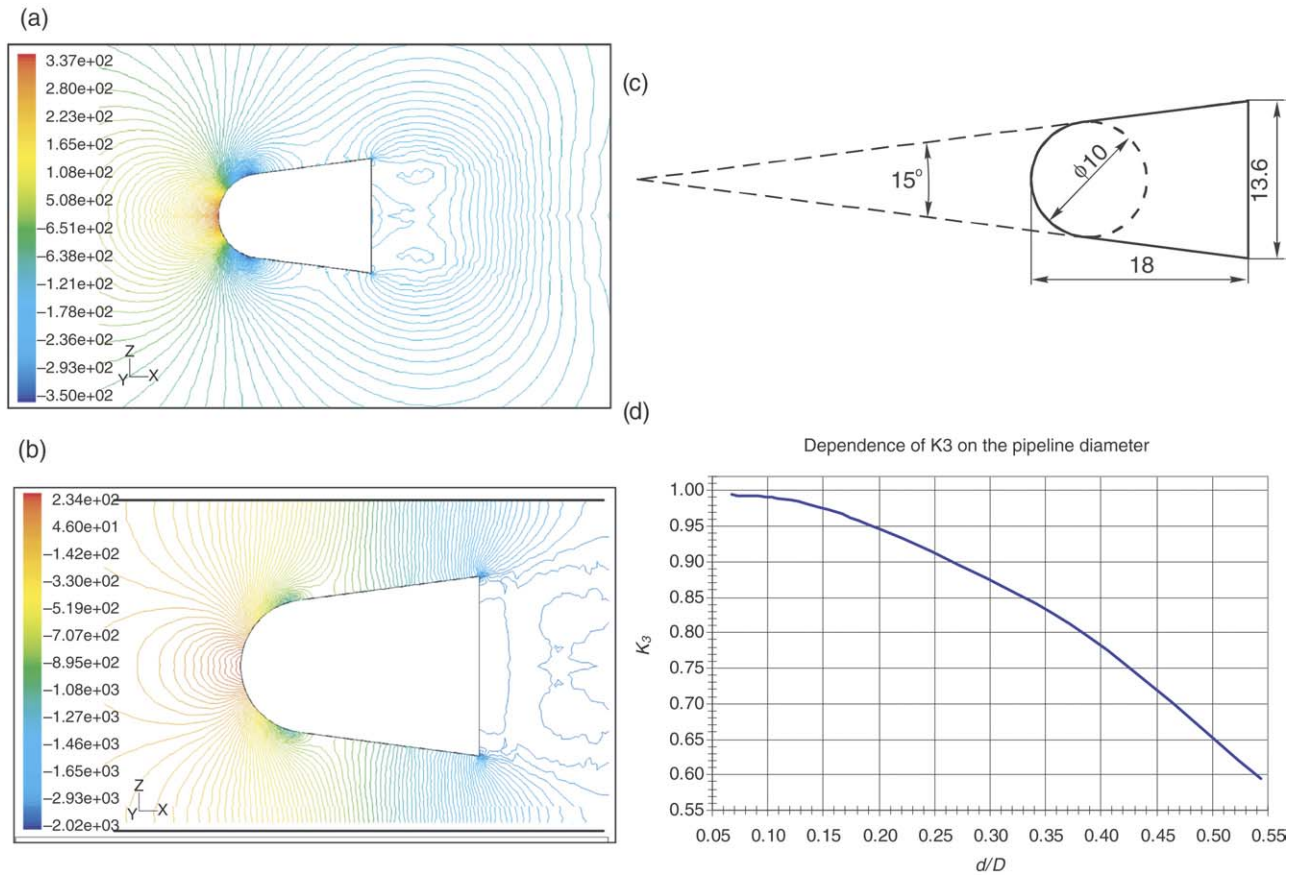Dependence of K3 on the pipeline diameter

Fig. 13. Values of K_3 including the effect of the streamline sensor in pipelines of diameters (a) $\phi 25$ mm, (b) $\phi 200$ mm; (c) sensor dimensions (in mm); (d) graph for pipeline diameters from the range 25–200 mm.
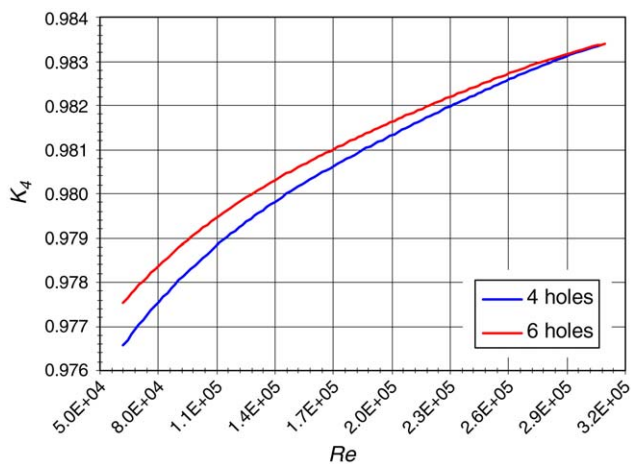

Fig. 14. Values of K_4 including a system of holes in the sensor.

Fig. 15. Error in determination of the air velocity, determined from the air compressibility.

5. Conclusions

Numerical solution of transport equations for the fluid and turbulence model allows one to analyse velocity and pressure fields in the neighbourhood of and inside the sensor. It also allows one to determine the correctness of
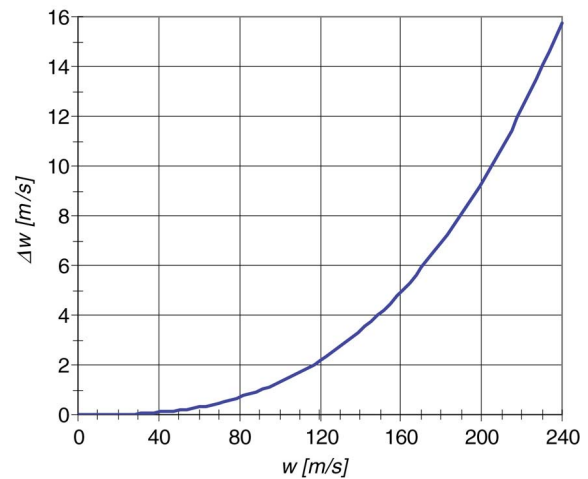
assumptions used for formulation of the sensor mathematical model, values and ranges of variability of the assumed coefficients.

The experimental results prove the quantitative correctness of the numerical results obtained. Numerical calcula-
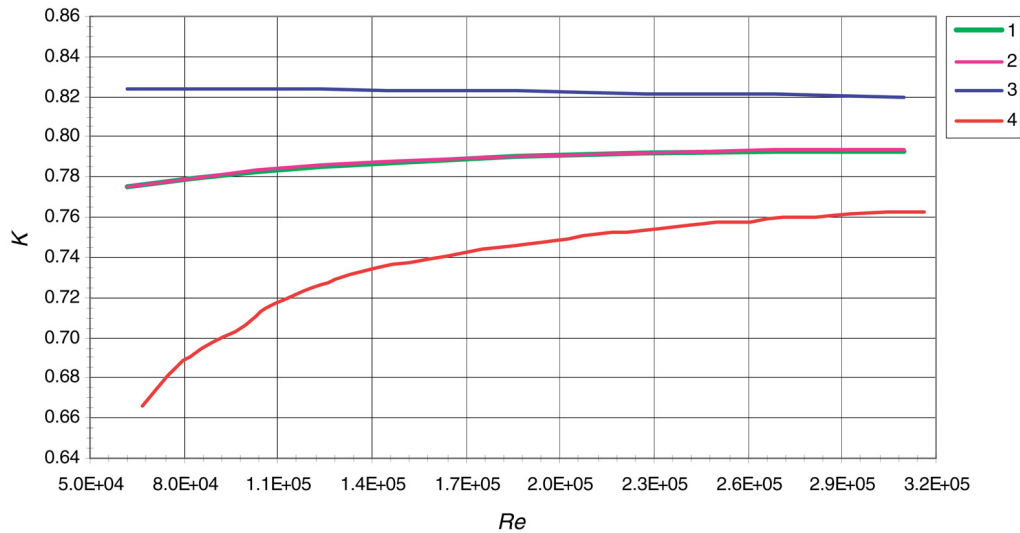
Fig. 16. Metrological characteristics of sensors with the following sections: 1—streamline (six holes on two sides), 2—streamline (four holes on each side), 3—streamline with small diameters of averaging chambers (ϕ2 mm is equal to the diameter of the impulse hole), 4—experimental data for the streamline sensor with six holes.

tions need, however, very dense meshes and the model must often be solved assuming that the case considered is unsteady.

The mathematical model formulated for the self-averaged Pitot tube includes relations between the flow coefficient K and many factors characterizing both sensor structure and flow. In the sensor all the factors can be distinguished. The sensor shape strongly influences K. The level of the pressure difference obtained and the variability of K with the flow change are strongly dependent on the shape. The blockage effect of the sensor on the stream is also very important—it causes increase of the measured pressure difference. It can be seen particularly when the pipeline diameter is lower than 125 mm. The influence of the impulse hole arrangement on K is not so strong (about 2%–4%). The hole arrangement is significant from the point of view of the measurement uncertainty.

Numerical simulations illustrate the influence of the averaging chamber size on the uniformity of the pressure distribution in the chambers. Application of chambers with section areas bigger than the impulse hole section areas influences the uniform pressure distribution in the chamber. The low diversification of pressures in the chambers on the outlet side shows that just one impulse hole can be used. This could lead to simplification of sensor manufacturing.

Application of the proposed methods to work on averaging impact sensors of new types with good metrological properties is described.

References

[1] J. Bouhy, Evolution of the Pitot tube sensor, in: Flow Metering Equipment, Preso, Ottawa, 1997.

[2] Dieterich, Standard Annubar – Flow Turndown and Differential Pressure Requirements – company publication, V, 1997.

[3] B. Dobrowolski, Z. Kabza, J. Pospolita, Theoretische und experimentelle Untersuchungen des Einflusses der Pulsationsstrtömung auf dis Charakteristiken der Drosselgeräte, VDI Verlag, Reihe 7: Strtömungstechnik, nr 193, Düsseldorf, 1992.

[4] B. Dobrowolski, Z. Kabza, Zastosowanie modelowania matematycznego i symulacji cyfrowej do analizy zjawiska przepływu przez zwężki, Postępy Technologii Maszyn i Urządzeń, nr 2, 1983.

[5] Fluent 6.0.20, Fluid Dynamics Analysis Package, Fluid Dynamics International, Inc., 2002.

[6] Gambit 2.0.4, Fluid Dynamics Analysis Package, Fluid Dynamics International, Inc., 2002.

[7] W.P. Graebel, Engineering Fluid Mechanics, Taylor & Francis Publishers, New York, London, 2001.

[8] W.H. Hickman, Annubar properties investigation, in: Proceedings of ISA's Industry Oriented Conference and Exhibit, vol. 30, Milwauke, 1975, s. 708 (1–14).

[9] ISO 5167, Measurement of fluid flow by means of pressure differential devices – cz. 1: Orifice plates, nozzles and Venturi tubes inserted in circular cross-section conducts running flow, 1991.

[10] M. Kabaciński, J. Pospolita, Numeryczne badania piętrzącego czujnika przepływu, Pomiary Automatyka Robotyka 4/2001.

[11] Z. Kabza, J. Pospolita, Analiza metrologiczna przepływomierzy z rurkami uśredniającymi ciśnienie dynamiczne, Krajowa Konferencja Metrologiczna, Warszawa, 1995.

[12] T.M. Kegel, Insertion (sampling) flow measurement, in: D.W. Spitzer (Ed.), w: Flow Measurement, Instrument Society of America, Research Triangle Park, 1991.

[13] S Kopacz, S. Waluś, Błędy niestałości uśredniających rurek spiętrzających, Zeszyty Naukowe Politechniki Śląskiej, Automatyka z.69, 1983.

[14] J.C.S. Lai, C.S. Yang, Numerical simulation of turbulence suppression: Comparisons of the performance of four k–ε turbulence models, International Journal of Heat and Fluid Flow 18 (1997) 575–584.

[15] T.M. Liou, Y.H. Hwang, L. Chen, Prediction of confined three-dimensional impinging flows with various turbulence models, Journal of Fluids Engineering 114 (1992) 220–230.

[16] G. Mompean, Numerical simulation of a turbulent flow near a right-angled corner using the speziale non-linear model with RNG k–ε equations, Computers & Fluids 27 (1998).

[17] S. Murakami, Overview of turbulence models applied in CWE – 1997, Journal of Wind Engineering and Industrial Aerodynamics (1998).

[18] C. Norberg, Flow around circular cylinder: aspects of fluctuating lift, Journal of Fluids and Structures 15 (2001).

[19] A. Petunin, Methods and technique of gas flow parameters measurement, Central Aerohydrodynamic Institute, CWA 22 Corporation, 2002.

[20] J. Pospolita, Przepływomierz różnicowo – ciśnieniowy do pomiaru w kanale o przekroju zamkniętym, Patent P 315387.

[21] J. Pospolita, The preliminary analysis of possibilities of the application of conventional flow-meters to measurements of unsteady flows, Archives of Hydro-Engineering and Environmental Mechanics, 1 - 4/1997.

[22] J. Pospolita, Theoretical evaluation of metrological properties of turbine flowmeters for measurement of pulsating flow, Archives of Hydroengineering XXXIX (4) (1992).

[23] W.J. Prosnak, Mechanika Płynów, tom I, PWN, Warszawa, 1970.

[24] R.S. Ransau, Simulation of flow around a three-dimensional circular cylinder utilizing computational mechanics software—ForcePAD, in: 15th Nordic Seminar of Computational Mechanics, 18–19 October 2002, Aalborg, Denmark, 2002.

[25] S. Rouvreau, L. Perault, Two-dimensional viscous vortex flow around a circular cylinder, Aerospace Science Technology V, 2001.

[26] T. Solberg, K.J. Eidsvik, Flow over a cylinder at a plane boundary—a model based upon $(k–\varepsilon)$ turbulence, Journal of Fluids Engineering 111 (1989) 414–419.

[27] P.R. Spalart, Strategies for turbulence modeling and simulations, International Journal of Heat and Fluid Flow II (2000).

[28] Turbulence Modelling: Part 2: Limitations of k–epsilon model, QNET CFD – LUZERN V, 2002.

[29] R.W.C.P. Verstappen, A.E.P. Veldman, Numerical computation of a viscous flow around a circular cylinder on a Cartesian grid, in: European Congress on Computational Methods in Applied Sciences and Engineering ECCOMAS, 2000.

[30] S. Waluś, Przepływomierze próbkujące; Pomiary, Automatyka, Robotyka, 2/1999.

[31] M. Wang, P. Catalano, G. Iaccarino, Prediction of high Reynolds number flow over a circular cylinder using LES with wall modelling, Center of Turbulence Research, Annual Research Briefs, 2001.